Turbo-Reception of OFDM with Coded M-DPSK

Peter Klenner and Karl-Dirk Kammeyer
Institute of Communications Engineering
University of Bremen, 28359 Bremen, Germany
Email: {klenner,kammeyer}@ant.uni-bremen.de

***Abstract*— Differential phase shift keying (DPSK) is an attractive modulation scheme in connection with OFDM as it circumvents channel estimation. However, it relies on strong correlation between adjacent symbols and is thus limited to those channels which exhibit either low frequency or low time selectivity. Based on previous works for the iterative improvement of DPSK in a broadband single-carrier context we present a turbo-receiver which exploits the concatenation of convolutional code, interleaver and DPSK modulation in a multi-carrier setting. We will show that our receiver provides vast improvements over simple differential demodulation with a performance close to or even surpassing standard coherent OFDM with MMSE channel estimation.**

***Index Terms*— Noncoherent Turbo-Detection, DPSK**

I. Introduction

MULTIPLE symbol differential detection (MSDD) [1] is commonly known as a means to improve the performance of DPSK. The basic idea is to extend the observation interval from two symbols as in conventional differential demodulation to a larger number of symbols. Within this extended interval a maximum-likelihood detection is performed. A number of recent papers brought this scheme into a turbo environment, e.g. in [2] linear prediction facilitates the implementation of approximate MAP-demodulation of DPSK. In [3] a similar receiver is developed for AWGN. Both these schemes are based on the application of an extended observation interval. In [4] this philosophy leads to a modified BCJR algorithm [5] whose metric follows directly from the joint probability of receive signal and transmit data and which is designed for minimum-shift keying modulation.

While these papers consider single carrier systems, this paper expands the ideas of [2], [3], [4] to OFDM with bit-interleaved convolutionally coded M-DPSK. Thereby our motivation is on the one hand to avoid explicit channel estimation and on the other hand to excel the performance of conventional differential detection of DPSK.

The paper is organized as follows. Section II describes the system model, Section III details the APP demodulation and the receiver's Turbo loop. Simulation results are presented in Section IV. Conclusions are given in Section V.

II. System model

Notation: Boldface lower-case characters denote vectors, e.g, $\mathbf{x}_a^b = [x_b, x_{b-1}, \cdots, x_a]^{\mathrm{T}}$, and boldface upper-case characters denote matrices, e.g, $\mathbf{X}$. The operator $\mathcal{D}\{\mathbf{x}\}$ places $\mathbf{x}$ on a diagonal matrix, $[\mathbf{X}]_{a,b}$ denotes a matrix element in the a-th row and b-th column, and $\mathrm{J}_0(\cdot)$ denotes the 0-th order modified Bessel function.

Throughout the paper we will consider differential modulation in frequency direction in order to enable demodulation on a per-OFDM-symbol-basis. Thus, for the following derivations we will omit an extra OFDM symbol index.

Fig. 1 depicts our transmitter. Independent identically-distributed information bits $b_i \in \{0,1\}$ are convolutionally encoded (CC) yielding code bits c_j. The randomly bit-interleaved sequence $c_{j'}$ is mapped onto M-ary DPSK symbols $\Delta d_n \in \{\exp(\mathrm{j}2\pi\xi/M), \xi = 0, \cdots, M-1\}$, which are differentially encoded according to the rule

$$d_n = \Delta d_n \cdot d_{n-1} \tag{1}$$

i.e., we chose to perform differential encoding in frequency direction. The block "reference symbols" provides the periodical initialization of the differential encoding process. An OFDM symbol in complex baseband notation is transformed into time domain by the IDFT

$$x_k = \frac{1}{\sqrt{N}} \sum_{\nu=0}^{N-1} d_\nu \mathrm{e}^{\mathrm{j}2\pi\nu k/N}, -N_{\mathrm{G}} \leq k \leq N-1, \tag{2}$$

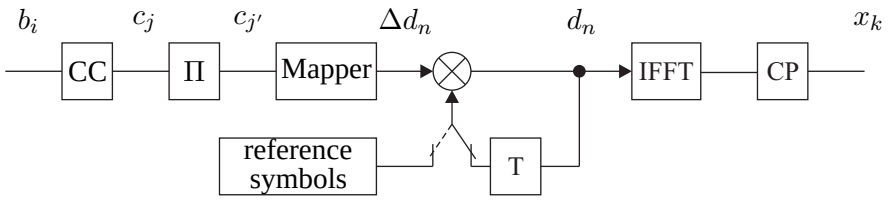

Fig. 1. OFDM transmitter

where N_{G} denotes the length of the cyclic prefix and N the number of subcarriers. Please note that x_k for $-N_{\mathrm{G}} \leq k \leq -1$ represents the cyclic prefix taken from the trailing end of the respective OFDM symbol.

The transmit signal x_k passes through a WSSUS time-variant multipath channel with impulse reponse $h_{\ell,k}$ (cf. [6]) and is superimposed by additive white Gaussian noise (AWGN) w_k with one-sided noise power spectral density N_0. The received signal in time domain is thus denoted as

$$y_k = \sum_{\ell=0}^{L-1} h_{\ell,k} x_{k-\ell} + w_k, \tag{3}$$

where L denotes the length of the channel impulse response. After removing the cyclic prefix and after discrete Fourier-transform the received OFDM symbol in the frequency domain is given by

$$r_n = \frac{1}{\sqrt{N}} \sum_{k=0}^{N-1} y_k \mathrm{e}^{-\mathrm{j}2\pi kn/N}. \tag{4}$$

For slowly time-varying channels this approach yields the most attractive property of OFDM, namely, the transformation of a multipath channel into a set of parallel flat-fading channels. Rapidly varying channels however lead to a loss of orthogonality and introduce intercarrier interference (ICI). Following the exposition in [7] we take ICI into account by modeling it as an additional noise term. Eq. (4) reads

$$r_n = \sum_{\nu=0}^{N-1} \sum_{\ell=0}^{L-1} d_\nu H_{\ell,\nu-n} \mathrm{e}^{-\mathrm{j}2\pi\nu\ell/N} + \eta_n \tag{5}$$

with

$$H_{\ell,\nu-n} = \frac{1}{N} \sum_{k=0}^{N-1} h_{\ell,k} \mathrm{e}^{\mathrm{j}2\pi k(\nu-n)/N} \tag{6}$$

and η_n for the DFT of the noise term w_k. Eq. (5) can be separated into a useful signal contribution, ICI and AWGN

$$r_n = \tilde{H}_n d_n + \tilde{w}_n, \tag{7}$$

where

$$\tilde{w}_n = c_n + \eta_n, \tag{8}$$

$$\tilde{H}_n = \sum_{\ell=0}^{L-1} H_{\ell,0} \mathrm{e}^{-\mathrm{j}2\pi n\ell/N}, \tag{9}$$

$$c_n = \sum_{\nu\neq n} \sum_{\ell=0}^{L-1} d_\nu H_{\ell,\nu-n} \mathrm{e}^{-\mathrm{j}2\pi\nu\ell/N}. \tag{10}$$

The ICI term c_n is assumed to be uncorrelated to the additive noise and to be distributed zero-mean Gaussian with variance (cf. [7, (10)])

$$\sigma_{\mathrm{ICI}}^2 = 1 - \frac{1}{N^2} \sum_{k=0}^{N-1} \sum_{k'=0}^{N-1} \mathrm{J}_0\left(2\pi f_{\mathrm{D,max}} T_s / N(k-k')\right) \tag{11}$$

which holds for Jakes' Doppler spectrum with maximum Dopppler frequency $f_{\mathrm{D,max}}$ and the OFDM core symbol duration T_s. Thus, $\tilde{w}_n \sim \mathcal{CN}(0, \sigma_{\mathrm{ICI}}^2 + \sigma_w^2)$ holds for the sum of ICI and AWGN. Let us further define the autocorrelation function

$$\varphi_{\tilde{H}\tilde{H}}(\lambda) \stackrel{\Delta}{=} \mathrm{E}\{\tilde{H}_n \tilde{H}_{n+\lambda}^*\} = (1-\sigma_{\mathrm{ICI}}^2) \sum_{\ell=0}^{L-1} \sigma_\ell^2 \mathrm{e}^{\frac{-\mathrm{j}2\pi\lambda}{N}} \tag{12}$$

with the ℓ-th path gain σ_ℓ^2.

III. APP Demodulation of M-DPSK

An APP demodulator basically needs to compute soft values for the coded and interleaved bits $c_{j'}$

$$\mathrm{L}(c_{j'}) = \log \frac{\sum_{\forall \Delta d_n(c_{j'}=0)} \Pr\left(\Delta d_n | \mathbf{r}_0^{N-1}\right)}{\sum_{\forall \Delta d_n(c_{j'}=1)} \Pr\left(\Delta d_n | \mathbf{r}_0^{N-1}\right)}. \tag{13}$$

Following the BCJR philosophy will render (13) into a computationally feasible expression. That approach was taken in [4]. Let us state the basic results. From (13) it is obvious that the main objective for an APP demodulator of DPSK is the computation of the a posteriori probability (APP) $\Pr\left(\Delta d_n | \mathbf{r}_0^{N-1}\right)$. Applying Bayes' rule this APP can be expressed as $\Pr\left(\Delta d_n | \mathbf{r}_0^{N-1}\right) = p\left(\Delta d_n, \mathbf{r}_0^{N-1}\right) / p\left(\mathbf{r}_0^{N-1}\right)$. Thus, the core of APP demodulation of DPSK is the computation of the joint probability $p\left(\Delta d_n, \mathbf{r}_0^{N-1}\right)$, which is well known from maximum a posteriori (MAP) decoding [5].

Let us first interprete the DPSK modulator as a trellis

encoder with a certain number of states and transitions. This trellis structure is purely artifical, i.e., the DPSK modulator remains a rate one recursive code, but the interpretation enables the expression of $p\big(\Delta d_n, \mathbf{r}_0^{N-1}\big)$ in terms of state transitions

$$p\big(\Delta d_n, \mathbf{r}_0^{N-1}\big) = \sum_{(s',s)\to\Delta d_n} p(s_n = s', s_{n+1} = s, \mathbf{r}_0^{N-1}). \tag{14}$$

In Eq. (14) the joint probability on the left hand side is expressed in terms of those state transitions (s', s) from state $s_n = s'$ to $s_n + 1 = s$ that belong to the considered differential transmit symbol Δd_n. For the following we will use the short hand notation $p(s', s, \mathbf{r}_0^{N-1}) = p(s_n = s', s_{n+1} = s, \mathbf{r}_0^{N-1})$. Repeatedly applying Bayes' rule leads to the computation of $p(s_n = s', s_{n+1} = s, \mathbf{r}_0^{N-1})$ in a forward-backward manner, i.e.,

$$p(s', s, \mathbf{r}_0^{N-1}) = \alpha_n(s')\gamma_n(s', s)\beta_{n+1}(s), \tag{15}$$

where the forward probability $\alpha_n(s')$, the transition probability $\gamma_n(s', s)$ and the backward probability $\beta_{n+1}(s)$ were introduced given by

$$\begin{aligned} \alpha_n(s') &= p(s', \mathbf{r}_0^{n-1}), & (16)\\ \gamma_n(s', s) &= p(r_n|s', s, \mathbf{r}_0^{n-1})\Pr(s|s'), & (17)\\ \beta_{n+1}(s) &= p(\mathbf{r}_{n+1}^{N}|s, \mathbf{r}_0^{n}). & (18) \end{aligned}$$

This approach becomes feasible due to the recursive update of the forward and backward probabilities

$$\begin{aligned} \alpha_{n+1}(s) &= \sum_{\forall s'\to\Delta d_n} \alpha_n(s')\gamma_n(s', s), & (19)\\ \beta_n(s') &= \sum_{\forall s\to\Delta d_n} \beta_{n+1}(s)\gamma_n(s', s). & (20) \end{aligned}$$

To actually compute these probabilities knowledge about the transition probability is required. Therefore we introduce

$$p(r_n|s', s, \mathbf{r}_0^{n-1}) = \frac{p(\mathbf{r}_0^n|s', s)}{p(\mathbf{r}_0^{n-1}|s', s)} \tag{21}$$

Recall that in Sec. II a subcarrier was described as being distorted by AWGN as well as ICI which was modeled by a zero-mean Gaussian distributed process. Hence, we can invoke the multivariate Gaussian distribution

$$p(\mathbf{r}_0^n|s', s) = \frac{\exp\left(-(\mathbf{r}_0^n)^{\mathrm{H}}\mathbf{C}_{rr}^{-1}[n]\mathbf{r}_0^n\right)}{\pi^{n+1}|\mathbf{C}_{rr}[n]|}, \tag{22}$$

where $\mathbf{C}_{rr}[n] = \mathrm{E}\{\mathbf{r}_0^n(\mathbf{r}_0^n)^{\mathrm{H}}|s', s\}$. Let

$$\mathbf{r}_0^n = \mathcal{D}\{\mathbf{d}_0^n\} \cdot \tilde{\mathbf{H}}_0^n + \tilde{\mathbf{w}}_0^n, \tag{23}$$

then the covariance matrix for $\mathbf{r}_0^n$ for M-DPSK is given by

$$\mathbf{C}_{rr}[n] = \mathcal{D}\{\mathbf{d}_0^n\}\left(\mathrm{E}\{\tilde{\mathbf{H}}_0^n(\tilde{\mathbf{H}}_0^n)^{\mathrm{H}}\} + \sigma_{\tilde{w}}^2\mathbf{I}\right)\mathcal{D}\{\mathbf{d}_0^n\}^{\mathrm{H}} \tag{24}$$

Inspection of Eq. (24) reveals that the determinant of $\mathbf{C}_{rr}[n]$ is independent of the transmitted data. Thus, replacing (22) in (21) yields

$$p(r_n|s', s, \mathbf{r}_0^{n-1}) \propto \frac{\exp\left(-(\mathbf{r}_0^n)^{\mathrm{H}}\mathbf{C}_{rr}^{-1}[n]\mathbf{r}_0^n\right)}{\exp\left(-\mathbf{r}_0^{n-1})^{\mathrm{H}}\mathbf{C}_{rr}^{-1}[n-1]\mathbf{r}_0^{n-1}\right)} \tag{25}$$

A direct implementation of Eq. (25) faces one significant problem. With increasing n the number of hypotheses and likewise the number of states increase, i.e., Eq. (25) entails a time-variant trellis. A remedy for this problem is inspired by the multiple-symbol detection approach of M-DPSK [1]. An observation interval is introduced, i.e., in Eq. (25) the conditioning on the total sequence $\mathbf{r}_0^{n-1}$ from 0 up until $n-1$ is replaced by the conditioning on $\mathbf{r}_{n-Z+1}^{n-1}$ which takes into account symbols from $n - Z + 1$ up to $n - 1$ yielding an approximation for the true conditional probability

$$p(r_n|s', s, \mathbf{r}_0^{n-1}) \approx p(r_n|s', s, \mathbf{r}_{n-Z+1}^{n-1}). \tag{26}$$

This approach eventually leads to approximate APPs in (14), however, iteratively including extrinsic information from the decoder will make up for this loss. The approximate conditional probability reads (cf. [4])

$$p(r_n|s', s, \mathbf{r}_{n-Z+1}^{n-1}) \propto \frac{\exp\left(-(\mathbf{r}_{n-Z+1}^n)^{\mathrm{H}}\tilde{\mathbf{C}}_{rr}^{-1}[n]\mathbf{r}_{n-Z+1}^n\right)}{\exp\left(-(\mathbf{r}_{n-Z+1}^{n-1})^{\mathrm{H}}\tilde{\mathbf{C}}_{rr}^{-1}[n-1]\mathbf{r}_{n-Z+1}^{n-1}\right)}. \tag{27}$$

The covariance matrices are given by

$$\begin{aligned} \tilde{\mathbf{C}}_{rr}[n] &= \mathrm{E}\left\{\mathbf{r}_{n-Z+1}^n(\mathbf{r}_{n-Z+1}^n)^{\mathrm{H}}|s', s\right\},\\ &= \mathcal{D}\{\mathbf{d}_{n-Z+1}^n\}\mathbf{C}_Z\mathcal{D}\{\mathbf{d}_{n-Z+1}^n\}^{\mathrm{H}} \end{aligned} \tag{28}$$

and

$$\begin{aligned} \tilde{\mathbf{C}}_{rr}[n-1] &= \mathrm{E}\left\{\mathbf{r}_{n-Z+1}^{n-1}(\mathbf{r}_{n-Z+1}^{n-1})^{\mathrm{H}}|s', s\right\}\\ &= \mathcal{D}\{\mathbf{d}_{n-Z+1}^{n-1}\}\mathbf{C}_{Z\text{-}1\times Z\text{-}1}\mathcal{D}\{\mathbf{d}_{n-Z+1}^{n-1}\}^{\mathrm{H}} \end{aligned} \tag{29}$$

with the definitions

$$\begin{aligned} \mathbf{C}_Z &= \mathrm{E}\{\tilde{\mathbf{H}}_{n-Z+1}^n(\tilde{\mathbf{H}}_{n-Z+1}^n)^{\mathrm{H}}\} + \sigma_{\tilde{w}}^2\mathbf{I}, & (30)\\ \mathbf{C}_{Z\text{-}1\times Z\text{-}1} &= \mathrm{E}\{\tilde{\mathbf{H}}_{n\text{-}Z+1}^{n\text{-}1}(\tilde{\mathbf{H}}_{n\text{-}Z+1}^{n\text{-}1})^{\mathrm{H}}\} + \sigma_{\tilde{w}}^2\mathbf{I}. & (31) \end{aligned}$$

The elements of the autocorrelation matrices are given by (12), i.e., $[\mathbf{C}_Z]_{\mu\nu} = [\mathbf{C}_{Z\text{-}1\times Z\text{-}1}]_{\mu\nu} =$

$\varphi_{\tilde{H}\tilde{H}}(\mu-\nu)+\sigma^2_{\tilde{w}}\delta_{\mu-\nu}$. In order to reduce the number of necessary computations in (27) we define

$$\mathbf{T} = -\mathbf{C}_Z^{-1} + \begin{pmatrix} 0 & \dots\ 0 \\ \vdots & \\ 0 & \mathbf{C}^{-1}_{Z-1\times Z-1} \end{pmatrix} \tag{32}$$

to eventually express (27) in the following quadratic form

$$\log p(r_n|s',s,\mathbf{r}_{n-Z+1}^{n-1}) \propto \tag{33}$$
$$(\mathbf{r}_{n-Z+1}^{n})^{\mathrm{H}}\mathcal{D}\{\mathbf{d}_{n-Z+1}^{n}\}\mathbf{T}\mathcal{D}\{\mathbf{d}_{n-Z+1}^{n}\}^{\mathrm{H}}\mathbf{r}_{n-Z+1}^{n}.$$

Noticing that $d_{n-b}d^*_{n-a}=\prod_{j=b}^{a-1}\Delta d_{n-j}$ and with $t_{\mu\nu} \triangleq [\mathbf{T}]_{\mu\nu}$, (33) is expressed in scalar notation as

$$\log p(r_n|s',s,\mathbf{r}_{n-Z+1}^{n-1}) \propto \tag{34}$$
$$2\cdot \mathrm{Re}\left\{\sum_{\mu=0}^{Z-1}\sum_{\nu=\mu+1}^{Z-1} t_{\mu\nu}r^*_{n-\mu}r_{n-\nu}\prod_{j=\mu}^{\nu-1}\Delta d_{n-j}\right\}.$$

Eq. (34) reveals the actual state and transition definitions. State $s_{n-1} = s'$ is associated with the hypothesis $\mathbf{\Delta d}_{n-Z+2}^{n-1}$, whereas the state transition (s',s) is described by the hypothesis for the actually transmitted differential symbol Δd_n.

Upon the recursive update of (19) and (20) using (34) we can compute (15) and arrive eventually at the soft values in (13). The extrinsic information for the differentially demodulated code bits is computed straightforwardly and after deinterleaving is fed into a standard BCJR decoder which decodes the convolutionally encoded bits. The extrinsic information of the code bits after decoding can then serve as a priori information in the next iterations.

IV. Simulation Results

Results in terms of BER simulations are presented for the WSSUS-channel with uniformly distributed power delay profile (channel taps $L = 3, 10$) and with Jakes' Doppler spectrum (normalized maximum Doppler frequencies $f_{\mathrm{D,max}}T_s = 0.01, 0.2$) corresponding to lowly/highly time/frequency-selective channels. The standard convolutional code $(133, 171)_8$ with random bit-interleaving and a block length of 10^4 information bits is applied. Our OFDM system uses $N = 64$ subcarriers and $N_{\mathrm{G}} = 16$ guard taps.

For a reference we simulated the coherent case with QPSK and perfect channel state information (CSI) with linear equalization (LE) and Viterbi decoding. The corresponding curves are marked as 'LE (ZF), perfect CSI' for zero-forcing equalization and 'LE (MMSE), perfect CSI' for MMSE equalization. Additionally we inserted simulation results for conventional differential demodulation, which bases the demodulation on two adjacent symbols. Decoding is again accomplished by the Viterbi algorithm. That case is marked by 'CDD'.

The performance of the Turbo receiver in Sec. III is marked either 'noncoh. Turbo APP (Gray)' for a Gray-mapped QDPSK or 'noncoh. Turbo APP (aGray)' for an anti-Gray-mapped QDPSK. Three iterations are performed. An observation interval of $Z = 5$ was chosen resulting in 64 states for the APP-demodulator. We added the case of a coherent OFDM system with channel estimation, i.e., following [8] several pilot symbols, which are known to the receiver, are distributed in the OFDM time-frequency grid. The pilots were spaced apart 3 symbols in frequency direction and 2 symbols in time direction. A 2-dimensional Wiener filter with 20 coefficients was implemented [8]. After estimating the channel at the pilot positions a subsequent interpolation based on the channel correlations yields the channel's transfer functions for all subcarriers. For this case we applied QPSK with an anti-Gray mapping. The Turbo loop is established between an optimal APP-demodulator and the BCJR-decoder for the convolutional code. Three iterations were performed, too. The curves are marked by 'coh. Turbo APP'.

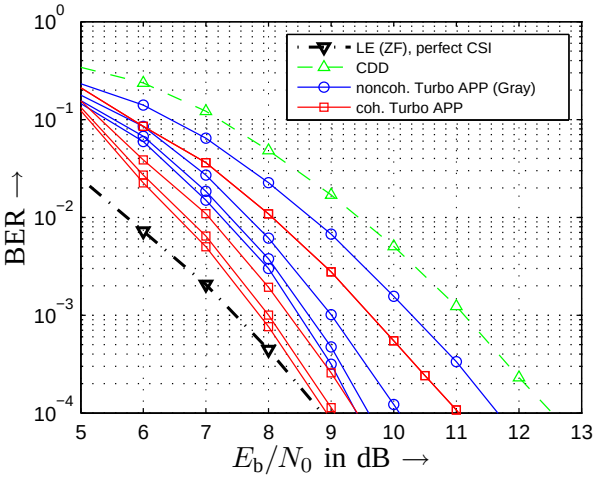

Fig. 2. Low time, low frequency selectivity, i.e., $f_{\mathrm{D,max}}T_s = 0.01$, $L = 3$ channel taps

In case of low time-selective channels (cf. Fig. 2,3) the *coherent* Turbo receiver is able to make up for the non-ideal channel estimation and can achieve the performance of the receiver which has perfect CSI. The *noncoherent* Turbo receiver achieves considerable gains against conventional differential demodulation but still leaves a gap to the perfect

CSI case of $\approx$ 0.5dB@10^{-4} for $L = 3$ and of $\approx$ 1.2dB@10^{-5} for $L = 10$.

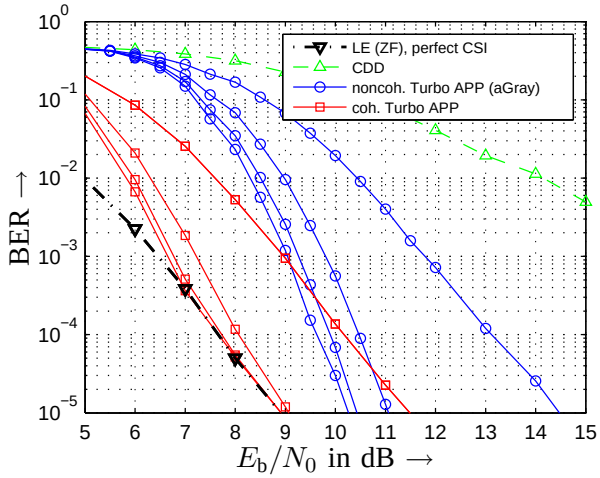

Fig. 3. Low time, high frequency selectivity, i.e., $f_{D,max}T_s = 0.01$, $L = 10$ channel taps

The situation becomes quite different for the rapidly changing channels. The normalized Doppler frequency $f_{D,max}T_s = 0.2$ leads to rapid channel variations which can not be reliably tracked by the pilot-aided channel estimator, i.e., the channel estimation fails due to a violation of the sampling theorem necessitating a denser pilot-grid. Fig. 4, 5 illustrate that the coherent Turbo receiver can only achieve a lowering of the error-floor.

On the other hand, for the rapidly fading but lowly frequency-selective channel the noncoherent Turbo receiver (Fig. 4) is able to almost achieve the performance of the perfect CSI case before it ends in an error-floor. Still at the highly frequency-selective channel the noncoherent Turbo receiver proves to be more robust than the coherent approach.

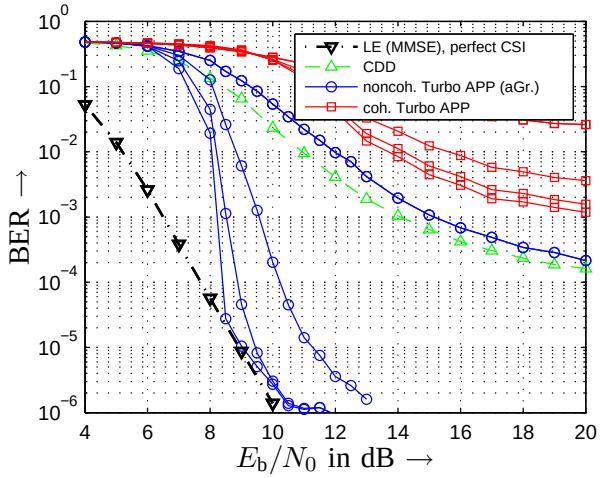

Fig. 4. High time, low frequency selectivity, i.e., $f_{D,max}T_s = 0.2$, $L = 3$ channel taps

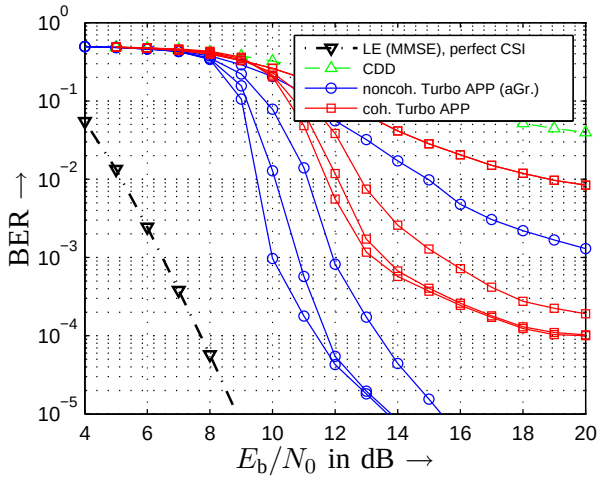

Fig. 5. High time, high frequency selectivity, i.e., $f_{D,max}T_s = 0.2$, $L = 10$ channel taps

V. Conclusion

We have successfully applied a modified BCJR algorithm [4] to the APP-demodulation of M-DPSK in an OFDM environment. We have shown the necessary changes for the BCJR demodulator. We have demonstrated that unlike coherent Turbo reception the noncoherent Turbo receiver proved to be robust for all considered channel conditions. As a final note let us mention that our noncoherent receiver achieves a lower error-floor with anti-Gray mapping whereas Gray-mapping results in an earlier beginning of the water-fall region.

References

[1] D. Divsalar, M. K. Simon, "Maximum-Likelihood Differential Detection of Uncoded and Trellis Coded Amplitude Phase Modulation Over AWGN and Fading Channels-Metrics and Performance", *IEEE Trans. Commun.*, vol. COM-42, pp. 76-89, January 1994

[2] P. Hoeher, J. H. Lodge, "Turbo DPSK": Iterative Differential PSK Demodulation and Channel Decoding, *IEEE Trans. Commun.*, vol. COM-47, pp. 837 - 843, June 1999

[3] I. D. Marsland, P. T. Mathiopoulos, "On the performance of iterative noncoherent detection of coded M-PSK signals", *IEEE Trans. Commun.*, vol. COM-48, pp. 588 - 596, April 2000.

[4] A. Hansson, T. Aulin; "Iterative diversity detection for correlated continuous-time Rayleigh fading channels", *IEEE Trans. Commun.*, vol. Com-51, pp. 240-246, Feb.2003

[5] L. R. Bahl, J. Cocke, F. Jelinek, J. Raviv, "Optimal decoding of linear codes for minimizing symbol error rate", *IEEE Trans. Inf.*, vol. 20, pp. 284-287, Mar. 1974

[6] P. Hoeher, "A Statistical Discrete-Time Model for the WSSUS Multipath Channel", *IEEE Trans. Com.*, vol. 41, no. 4, Nov. 1992

[7] M. Russell, G. L. S. Stüber, "Interchannel interference analysis of OFDM in a mobile environment", *Proc. VTC'95*, Chicago, IL, July 1995, pp. 820–824.

[8] P. Hoeher, S. Kaiser, and P. Robertson, "Two-Dimensional Pilot-Symbol-Aided Channel Estimation by Wiener Filtering", *ICASSP*, vol.3, pp. 1845-1848, April 1997